

---

# Rethinking Vector Field Learning for Generative Segmentation

---

Chaoyang Wang<sup>1,2</sup> Yaobo Liang<sup>1</sup> Boci Peng<sup>1</sup> Fan Duan<sup>2</sup>  
Jingdong Wang<sup>2</sup> Yunhai Tong<sup>1</sup>  
<sup>1</sup>Peking University <sup>2</sup>Baidu  
cywang@stu.pku.edu.cn

## Abstract

Taming diffusion models for generative segmentation has attracted increasing attention. While existing approaches primarily focus on architectural tweaks or training heuristics, there remains a limited understanding of the intrinsic mismatch between continuous flow matching objectives and discrete perception tasks. In this work, we revisit diffusion segmentation from the perspective of vector field learning. We identify two key limitations of the commonly used flow matching objective: gradient vanishing and trajectory traversing, which result in slow convergence and poor class separation. To tackle these issues, we propose a principled vector field reshaping strategy that augments the learned velocity field with a detached distance-aware correction term. This correction introduces both attractive and repulsive interactions, enhancing gradient magnitudes near centroids while preserving the original diffusion training framework. Furthermore, we design a computationally efficient, quasi-random category encoding scheme inspired by Kronecker sequences, which integrates seamlessly with an end-to-end pixel neural field framework for pixel-level semantic alignment. Extensive experiments consistently demonstrate significant improvements over vanilla flow matching approaches, substantially narrowing the performance gap between generative segmentation and strong discriminative specialists.

## 1 Introduction

Diffusion models [34, 35, 16] have emerged as a leading approach in visual generation, excelling at modeling complex data distributions. Their effectiveness in high-quality image synthesis [32, 30, 12], video generation [4, 1, 15] and image editing [5] has motivated extensions to various downstream tasks. While initially proposed for visual generation, recent works [44, 38, 37] have begun applying diffusion frameworks to perception tasks, aiming to unify generation and understanding within a common paradigm. Among these tasks, segmentation is distinctive in that it assigns each pixel a discrete semantic label [29, 8, 33, 48, 11, 10], producing categorical rather than continuous outputs. This poses a key challenge: diffusion models operate in continuous spaces, while segmentation requires inherently discrete predictions. This gap introduces significant challenges in task formulation and optimization.

To adapt diffusion models for segmentation and utilize their pretrained priors, existing methods fall into three main categories, as shown in Fig. 2. 1) Using diffusion models as feature extractors with segmentation heads [49, 42, 20, 17, 36, 3, 18]. 2) Employing visual foundation features and adding lightweight diffusion modules to refine masks [39, 14, 13]. 3) Treating segmentation as end-to-end image translation, encoding masks as three-channel pseudo-color images [2, 21, 37, 38, 31, 24]. Beyond model design, interestingly, semantic segmentation remains a challenging and underexplored task for diffusion-based models, primarily due to two factors: 1) the mismatch between the inherent

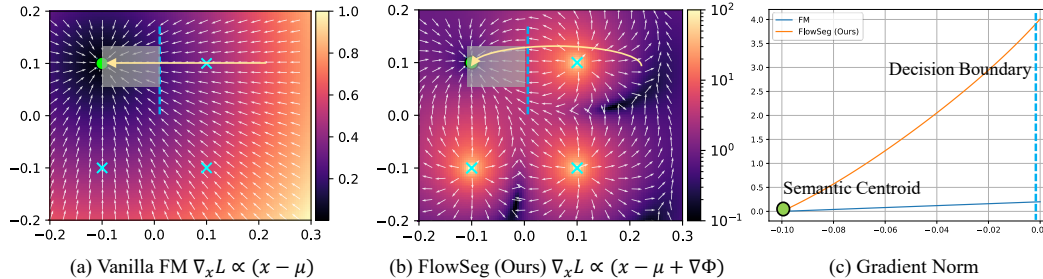


Figure 1: **Visualization of gradient vanishing and trajectory traversing in generative segmentation (x-prediction).** (a) Vanilla flow matching suffers from vanishing gradients near semantic centroids  $\mu$ , resulting in slow and non-discriminative trajectories that may traverse proximal neighborhoods of competing centroids and cause false predictions. (b) FlowSeg (ours) introduces a potential function  $\Phi$  to enhance gradients around target centroids and enforce repulsion from non-targets, enabling faster convergence and more discriminative, deflected trajectories. The  $x - \mu$  term maintains convergence near outer boundaries. (c) Gradient norm from centroid to decision boundary (gray regions in (a),(b)): Our method maintains strong gradients, whereas vanilla flow matching gradients nearly vanish. Yellow curves and blue dashed lines denote the predicted trajectory and decision boundary; the green dot marks the target centroid, and blue crosses indicate irrelevant categories.

stochasticity of generative models and the deterministic demands of semantic segmentation, and 2) the typically large number of classes involved. Recent works [38, 21] address the first challenge by introducing deterministic flows, yet the issue of high class cardinality persists. To maintain tractability, existing approaches often simplify the problem setting. For instance, some methods reduce the class space by merging similar categories [43], or reformulate the task as a series of referring image segmentation problems [14] to break it into simpler subproblems. These findings indicate that stochasticity and high class cardinality are fundamental obstacles for diffusion segmentation, suggesting that the core difficulty lies not in model capacity, but in the optimization dynamics inherent to the framework.

In this paper, we analyze the issue from an optimization dynamics perspective and identify two key problems: *gradient vanishing* and *trajectory traversing*, as shown in Fig. 1. By examining the gradients induced by standard flow matching [25, 26], we observe that the optimization signal is directly scaled by the distance between predictions and semantic centroids. As class centroids reside in a bounded low-dimensional space, the gradients are inherently limited and decay rapidly as predictions approach the target, ultimately vanishing near convergence and causing optimization to stall. Furthermore, the regression-based approach only provides attractive forces toward the ground-truth class, lacking explicit repulsion from competing centroids. This combination of weak gradients and absent inter-class repulsion results in slow convergence and poor semantic separation, ultimately degrading segmentation performance.

To overcome these limitations, we reshape the vector field by introducing a distance-aware correction term to the original velocity, enabling both attractive and repulsive interactions and sustaining non-vanishing gradients near centroids. This enhances class separation and accelerates convergence. Additionally, we propose a quasi-random centroid encoding strategy inspired by Kronecker sequences, which is computationally efficient. Combined with an end-to-end pixel neural field framework, our design aligns the diffusion model with pixel-level tasks.

Our main contributions are summarized as follows: 1) We analyze the slow convergence and suboptimal performance in diffusion segmentation, attributing them to gradient vanishing and trajectory traversing caused by the vanilla flow matching objective. 2) We propose a novel vector field reshaping strategy that augments target velocity with a corrective term, preserving gradient magnitude and introducing explicit repulsion to improve semantic separation. 3) We employ a pixel neural field framework for end-to-end training and introduce a scalable, quasi-random centroid encoding scheme that ensures balanced inter-class geometry without extra optimization. 4) Extensive experiments show consistent and significant improvements, substantially narrowing the gap between generative and strong discriminative approaches.

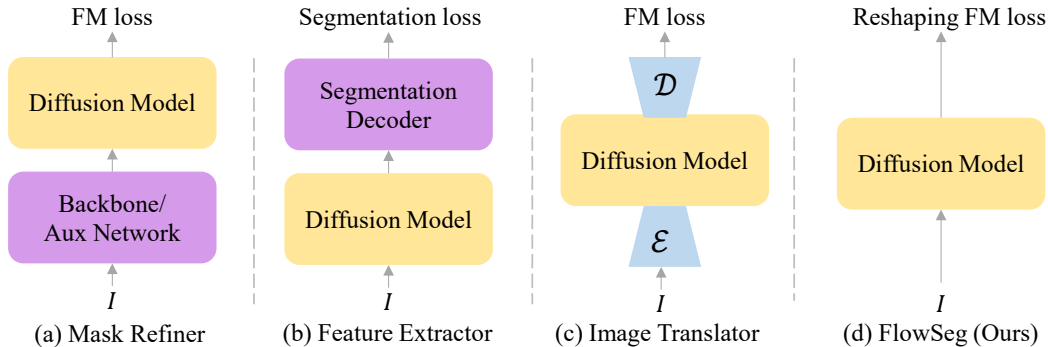


Figure 2: **Comparison of diffusion segmentation paradigms.** (a) Diffusion models are used primarily for mask refinement, relying on an external backbone for feature extraction or auxiliary networks for coarse segmentation. (b) Diffusion models serve as the backbone, followed by a dedicated segmentation head. (c) The segmentation task is formulated as image-to-mask translation without auxiliary networks, yet still depends on a pretrained VAE. (d) FlowSeg (ours) performs pixel-level end-to-end training without additional auxiliary modules, and rectifies vanilla flow matching by reshaping the underlying vector field for better optimization. Noise is omitted for simplicity.

## 2 Related Work

### 2.1 Diffusion and Flow

Diffusion models [16] and flow models [25, 27] parameterize data generation as a time-dependent dynamical system that transports a simple reference distribution to a target data distribution. They enable high-fidelity synthesis across diverse domains, including image generation [32, 30, 12], video generation [4, 1, 15], image editing [5], etc. Early diffusion models typically use stochastic differential equations (SDEs) to learn score or noise estimates under a predefined Gaussian corruption process. In contrast, flow models [27, 28] directly learn a deterministic velocity field that defines a straight probability path, enabling more efficient sampling and greater flexibility in distribution transport.

To reduce computational overhead, conventional approaches [32] predominantly operate within latent spaces compressed by Variational Autoencoders (VAEs) [19]. However, the inherent information loss in VAE compression often hinders tasks that require pixel-level precision and direct spatial alignment. To address this, recent pixel diffusion models [46, 22, 40] have emerged, leveraging large patch decoding to maintain scalability without sacrificing fine-grained details. Despite differences in parameterization, these approaches share a common principle: generative modeling is reduced to learning a *continuous* vector field that aligns probability trajectories between distributions, typically via regression-based objectives, which poses a challenge for extending to *discrete* perception tasks.

### 2.2 Generative Segmentation

Visual segmentation aims to partition an image into semantically coherent regions with discrete class labels. While conventional methods [29, 8, 33, 48, 11, 10] typically frame segmentation as a discriminative dense classification task, generative formulations have recently gained traction for their superior uncertainty modeling and structured prediction capabilities [2, 23].

Existing diffusion segmentation methods generally follow three paradigms: 1) Feature-based, which utilize diffusion backbones as powerful frozen extractors for task-specific segmentation heads [49, 42, 20, 17, 36, 3, 18]; 2) Refinement-based, which employ diffusion modules to iteratively polish masks generated by foundation models [39, 14, 13]; 3) Unified-generative, which cast mask prediction as an end-to-end image translation process [2, 21, 37, 38, 31, 24].

In the unified-generative formulation, segmentation masks are typically embedded into a low-dimensional continuous manifold to align with the continuous nature of generative dynamics. While such embedding is essential for generative modeling, simply adopting vanilla regression-based flow objectives fails to account for the discrete nature of semantic labels. This leads to an optimization

mismatch where the vector field is learned as a generic density estimator, overlooking the categorical constraints inherent in segmentation.

### 3 Optimization Dynamics Analysis

In this section, we provide a formal analysis of why the standard Mean Squared Error (MSE) objective, commonly used in Flow Matching for generative tasks, leads to suboptimal optimization dynamics and performance bottlenecks when applied to generative segmentation.

#### 3.1 Preliminary

Let  $I \in \mathbb{R}^{H \times W \times 3}$  denote an input image. We define the segmentation task as a flow between a source distribution  $p_0(x_0|I)$  and a target distribution  $p_1(x_1)$ . To eliminate the randomness of Gaussian noise and leverage the deterministic nature of segmentation, we define  $x_0$  as a feature-dependent distribution (e.g., the input image itself or encoded image features) and  $x_1$  as the target mask representation.

In a categorical or multi-channel segmentation setting, each pixel or region is mapped to a specific target centroid within a bounded continuous space (e.g.,  $\mathcal{C} \subset [-1, 1]^d$ ). Let  $\mathcal{P} = \{\mu_1, \mu_2, \dots, \mu_N\}$  be the set of target centroids representing  $N$  distinct categories or instances. In Rectified Flow [27], the probability path  $x_t$  is constructed as follows:

$$x_t = (1-t)x_0 + tx_1, \quad t \in [0, 1] \quad (1)$$

The corresponding ground-truth velocity (vector field) is:

$$v_{gt}(x_t) = \frac{dx_t}{dt} = x_1 - x_0 \quad (2)$$

The standard training objective is to learn a velocity field  $v_\theta(x_t, t, I)$  parameterized by a neural network, which approximates the ground-truth via the MSE loss:

$$\mathcal{L}_{FM} = \mathbb{E}_{t, x_0, x_1} \|v_\theta(x_t, t, I) - v_{gt}\|^2 \quad (3)$$

#### 3.2 Gradient Analysis

To understand the optimization challenges, we analyze the gradient of  $\mathcal{L}_{FM}$  with respect to the network’s prediction. The velocity  $v_\theta$  implicitly defines a predicted target  $\hat{x}_1$ , which can be estimated as:

$$\hat{x}_1 = x_t + (1-t)v_\theta \quad (4)$$

Substituting  $v_\theta$  and  $v_{gt}$  into the loss function, we can rewrite the objective in terms of the distance between the predicted state and the target centroid:

$$\mathcal{L}_{FM} \propto \left\| \frac{\hat{x}_1 - x_t}{1-t} - \frac{x_1 - x_t}{1-t} \right\|^2 = \frac{1}{(1-t)^2} \|\hat{x}_1 - x_1\|^2 \quad (5)$$

By examining the gradient of this loss with respect to the predicted target  $\hat{x}_1$ , several critical issues emerge regarding the optimization dynamics:

**Gradient Vanishing Near Centroids.** The gradient magnitude is directly proportional to the Euclidean distance between the prediction and the target for fixed  $t$ :

$$\nabla_{\hat{x}_1} \mathcal{L}_{FM} \propto (\hat{x}_1 - x_1) \quad (6)$$

As the prediction  $\hat{x}_1$  approaches the target centroid  $x_1 \in \mathcal{P}$ , the gradient vanishes. In the late stages of training, the model lacks sufficient driving force to precisely converge to the exact centroid coordinates, leading to blurry segmentation boundaries.

**Limited Signal Scale in Bounded Space.** Given that the centroids  $\mathcal{P}$  are typically embedded in a compact space such as  $[-1, 1]^d$ , the maximum possible distance  $\|\hat{x}_1 - x_1\|$  is intrinsically small. For tasks with high category cardinality  $N$ , the centroids are densely packed, and the MSE-based gradient provides a very weak signal for the model to distinguish between adjacent categorical anchors.

**Absence of Repulsive Forces.** The MSE loss is strictly a *unimodal attraction* objective. It solely penalizes the distance to the target centroid and remains agnostic to competing centroids. On the

one hand, from the perspective of classical contrastive learning, a robust classifier should not only pull the prediction toward the positive category but also push it away from negative ones. On the other hand, from the perspective of flow matching, without a repulsive mechanism, target-bound trajectories may inadvertently *traverse* the proximal neighborhoods of competing classes, inducing semantic ambiguity during the generative process.

## 4 Method

In this section, we detail the proposed framework to rectify the optimization dynamics of generative segmentation. First, we introduce a deterministic, quasi-random scheme for category encoding. Then, we present the vector field reshaping mechanism, which is designed to introduce discriminative forces into the generative training objective. Finally, we propose using pixel neural field decoding for end-to-end generative segmentation training.

### 4.1 Category Encoding

To map  $N$  semantic categories into the bounded 3D color space  $\mathcal{C} \subset [-1, 1]^3$ , we employ a Kronecker-style sequence based on algebraically independent increments, which is a quasi-random sequence characterized by determinism and low computational cost.

Let  $\mathcal{V} = \{\sqrt{2}, \sqrt{3}, \sqrt{5}\}$  be a set of square roots of the first three primes. These values are linearly independent over the field of rational numbers  $\mathbb{Q}$ , ensuring that the generated sequence does not collapse onto lower-dimensional manifolds or exhibit periodic correlations. For each category index  $k \in \{0, \dots, N-1\}$ , the centroid  $\mu_k$  is initially computed as:

$$\hat{c}_k = (k \cdot \mathcal{V}) \pmod{1} \quad (7)$$

The resulting coordinates are then normalized and stretched to occupy the full volume of the  $[-1, 1]^3$  cube:

$$\mu_k = 2 \cdot \text{Norm}(\hat{c}_k) - 1 \quad (8)$$

This approach ensures a relatively uniform distribution of centroids with high minimum inter-point distances, providing a stable and deterministic geometric basis for the vector field learning.

### 4.2 Vector Field Reshaping

As analyzed in Sec. 3, the vanilla flow matching objective fails to provide repulsive forces, leading to path traversing and gradient vanishing. To address this, we reshape the flow matching objective by augmenting the ground-truth velocity  $v_{gt}$  with a discriminative rectification term.

**Potential-based Vector Rectification.** To instill discriminative awareness into the flow field, we construct a potential field  $\Phi$  over the centroid space. Let  $\hat{x}_1$  denote the estimated prediction, and  $d_k = \|\hat{x}_1 - \mu_k\|^2$  be the squared Euclidean distance to target centroid  $\mu_k \in \mathcal{P}$ . We introduce a transformation operator  $\mathcal{T}(\cdot)$  to map these geometric distances into a semantic embedding space. In our primary formulation, we define this operator as  $\mathcal{T}(d) = -\log(d + \epsilon)$ , where  $\epsilon$  is to avoid zero-division.  $\mathcal{T}$  remains flexible for various distance-warping strategies.

Distances are converted into a soft-assignment distribution  $p$  via a temperature-scaled softmax over the transformed distances:

$$p_k = \frac{\exp(\mathcal{T}(d_k)/\tau)}{\sum_j \exp(\mathcal{T}(d_j)/\tau)} \quad (9)$$

where  $\tau$  is a temperature hyperparameter controlling the sharpness of the categorical assignment. To guide the optimization, we define the discriminative potential  $\Phi$  as the divergence between the current assignment  $p$  and the ground-truth one-hot distribution  $y$ :

$$\Phi(\hat{x}_1, y) = -\sum_{k=1}^N y_k \log p_k \quad (10)$$

This potential reaches its global minimum when the prediction  $\hat{x}_1$  perfectly aligns with the target centroid  $\mu_{gt}$  while maximizing its separation from competitors. The rectification term  $\nabla \Phi$  is obtained

by computing the gradient of the potential with respect to the prediction  $\hat{x}_1$ . Utilizing the property  $\mathcal{T}'(d) = -(d + \epsilon)^{-1}$ , the gradient is formulated as:

$$\nabla\Phi = \frac{\partial\Phi}{\partial\hat{x}_1} = \frac{2}{\tau} \sum_{k=1}^N (y_k - p_k) \frac{\hat{x}_1 - \mu_k}{d_k + \epsilon} \quad (11)$$

**Objective Reformulation.** The reshaped target velocity  $\tilde{v}_t$  is defined by integrating the rectification term into the original velocity:

$$\tilde{v}_t = v_t - \nabla\Phi \quad (12)$$

To maintain the stability of the probability path and prevent the network from directly optimizing the potential field, we apply the stop-gradient operator to the reshaped target. The final training objective is defined as:

$$\mathcal{L}_{res} = \mathbb{E}_{t, x_0, x_1} \|v_\theta(x_t, t, I) - \text{sg}[\tilde{v}_t]\|^2 \quad (13)$$

where  $\text{sg}[\cdot]$  denotes the detach operation.

**Gradient Dynamics Comparison.** To further elucidate the impact of Flow Reshaping, we compare the gradients of the standard Flow Matching loss and our proposed objective. For the sake of clarity, let  $g_\theta = \nabla_\theta v_\theta$  denote the Jacobian of the network with respect to its parameters.

In the standard Flow Matching framework, the parameter update is driven by:

$$\nabla_\theta \mathcal{L}_{FM} = g_\theta^\top (v_\theta - (x_1 - x_0)) \quad (14)$$

As  $v_\theta$  approaches the constant target  $v_{gt} = x_1 - x_0$ , the error signal diminishes. This signal is purely reconstructive, providing no information regarding the proximity of the predicted flow to incorrect categorical centroids.

In contrast, our reshaped objective  $\mathcal{L}_{res}$  yields the following gradient:

$$\nabla_\theta \mathcal{L}_{res} = g_\theta^\top (v_\theta - (x_1 - x_0 - \text{sg}[\nabla\Phi])) \quad (15)$$

By decomposing the term  $\nabla\Phi$ , we observe that a discriminative bias shifts the effective target for the network:

$$\text{Effective Target} = \underbrace{(x_1 - x_0)}_{\text{Reconstructive}} + \underbrace{\frac{2}{\tau} \sum_{k=1}^N (p_k - y_k) \frac{\hat{x}_1 - \mu_k}{\|\hat{x}_1 - \mu_k\|^2 + \epsilon}}_{\text{Discriminative Correction}} \quad (16)$$

*Discussion.* Superiority of the reshaped vector field:

1) Adaptive Repulsion: Unlike the standard objective where the target is a static vector, our correction term is a weighted sum of vectors pointing away from all centroids. When the flow  $v_\theta$  inadvertently directs the prediction toward an incorrect centroid  $\mu_j$  ( $j \neq gt$ ), the term  $p_j \frac{\hat{x}_1 - \mu_j}{d_j}$  increases, effectively warping the target velocity to steer the trajectory away from the competitor.

2) Mitigation of Gradient Vanishing: As analyzed in Section 3.2, standard flow matching gradients vanish near the target centroid. In our formulation, the term  $(p_{gt} - 1) \frac{\hat{x}_1 - \mu_{gt}}{d_{gt}}$  provides a normalized attraction force. Since  $p_{gt} < 1$ , the term  $(p_{gt} - 1)$  maintains a significant magnitude even when the prediction is close to the centroid, ensuring the model continues to optimize.

3) Optimization Dynamics: By incorporating the  $\text{sg}[\cdot]$  operator, we avoid the instabilities associated with second-order gradients of the potential field. The network learns to approximate a reshaped velocity field that is inherently aware of the decision boundaries in the centroid space, transforming the flow from simple interpolation to discriminative transport.

### 4.3 End-to-End Pixel Decoding

Conventional VAE-based latent spaces are often ill-suited for high-precision segmentation due to *manifold distortion* and *optimization decoupling*. The former introduces latent artifacts that disrupt pixel-level details, while the latter prevents the diffusion process from aligning directly with segmentation objectives. Moreover, the high memory overhead of VAEs makes full end-to-end optimization computationally infeasible.

To circumvent these limitations, following PixNerd [40], we propose using pixel neural field decoding for end-to-end generative segmentation training. Instead of decoding a patch feature  $\mathbf{X}^n \in \mathbb{R}^D$  through a simplistic linear projection, we treat each patch as a continuous neural field. The Transformer backbone serves as a parameter generator, predicting the weights of a localized Multi-Layer Perceptron (MLP). For the  $n$ -th patch, the network dynamically predicts the weight matrices  $\{\bar{\mathbf{W}}_1^n, \bar{\mathbf{W}}_2^n\}$  of a lightweight MLP from the patch feature. These weights are generated via a non-linear projection and subsequently  $L_2$ -normalized to ensure numerical stability, yielding the normalized weights  $\mathbf{W}_1^n$  and  $\mathbf{W}_2^n$ :

$$\mathbf{W}_1^n, \mathbf{W}_2^n = \text{Linear}(\mathbf{X}^n)$$

To query the velocity field at any spatial coordinate  $(i, j)$  within the patch, we construct an input context  $\mathbf{h}_{i,j}$  by concatenating the Discrete Cosine Transform (DCT) positional encoding with the noisy pixel state  $\mathbf{x}_t(i, j)$ :

$$\mathbf{h}_{i,j} = \text{Concat}([\text{DCT}(i, j), \mathbf{x}_t(i, j)])$$

The final pixel-wise velocity  $v^n(i, j)$  is then directly decoded by applying the dynamically generated MLP:

$$v^n(i, j) = \bar{\mathbf{W}}_2^n \sigma(\bar{\mathbf{W}}_1^n \mathbf{h}_{i,j})$$

where  $\sigma$  denotes the SiLU activation function.

## 5 Experiment

In this section, we first introduce our experimental settings and then compare them with baseline methods quantitatively and qualitatively. Finally, we provide ablation studies for different modeling strategies, convergence comparisons, and generative property analysis.

### 5.1 Experimental Settings

**Dataset.** We evaluate our approach on two high-cardinality datasets: ADE20K [50] and COCO-Stuff [6]. ADE20K is a scene parsing dataset covering 150 fine-grained semantic concepts consisting of 20k images. COCO-Stuff covers 171 labels and consists of 164k images.

**Implementation.** Our model is initialized with PixNerd [40] weights. All images and segmentation masks are resized to a uniform resolution. Training proceeds in two progressive stages, using the AdamW optimizer and Representation Alignment (REPA) [45] to accelerate convergence. Stage 1 uses a  $256 \times 256$  resolution with a batch size of 64, followed by Stage 2 at  $512 \times 512$  with a batch size of 16. The default temperature is 1.0. In line with standard practice, binary masks are applied to filter out unlabeled regions, which are omitted from our notation for brevity.

**Baselines.** We consider discriminative specialists and diffusion models in our experiments. For discriminative specialists, we include DeeplabV3+ [9], OCRNet [47], SegFormer [41] and MaskFormer [11]. For diffusion models, we include InstructDiffusion [14], PixWizard [24] and SymmFlow [7]. Note that some diffusion-based methods adopt a similar task, referring image segmentation. It is similar to semantic segmentation, but transforms *one* high-cardinality classification problem into *multiple* binary classification problems, and uses a text prompt for assistance, which would be advantageous compared to standard semantic segmentation.

### 5.2 Main Results

**Quantitative results.** We compare our methods with discriminative specialists and diffusion-based generative segmentation models in Tab. 1a and Tab. 1b, respectively. Overall, diffusion models perform worse than discriminative models by a remarkable margin, even when initialized with Stable Diffusion [32], which is pretrained on large-scale text-image pair datasets and has rich world knowledge. This discrepancy underscores the inherent challenges of generative segmentation for diffusion frameworks, aligning with our analysis in Sec. 3. In particular, on the ADE20K dataset, InstructDiffusion and PixWizard fall behind DeepLabV3+ with 10.5 and 11.3 mIoU, respectively. On the COCO-Stuff dataset, a similar trend persists: even when initialized with a powerful SD2.1, SymmFlow still falls behind SegFormer by 5 mIoU. Thanks to the reshaped vector field learning, our proposed FlowSeg achieves promising results, with mIoU of 47.1 and 44.9 on both ADE20K and

Table 1: **Comparisons on ADE20K and COCO-Stuff dataset.** † indicates that it performs referring image segmentation, which requires predicting a separate mask for each semantic category. LSTI and (·) indicate large-scale text-image datasets and the initialized weight, respectively. **Bold** and underline indicate the first and second best entries.

(a) Performance on ADE20K dataset				
	Method	Backbone	Pretrain Data	mIoU
Discriminative Specialists	DeeplabV3+	ResNet101	IN-1k	44.1
	SegFormer	MiT-B2	IN-1k	46.5
	MaskFormer	Swin-T	IN-1k	<u>46.7</u>
Diffusion Models	InstructDiffusion†	(SD1.5)	LSTI	33.6
	PixWizard	(Lumina-Next-T2I)	LSTI	32.8
	FlowSeg (Ours)	(PixNerd)	IN-1k	<b>47.1</b>

(b) Performance on COCO-Stuff dataset				
	Method	Backbone	Pretrain Data	mIoU
Discriminative Specialists	DeeplabV3+	ResNet50	IN-1k	38.4
	OCRNet	HRNet-W48	IN-1k	42.3
	SegFormer	MiT-B2	IN-1k	<u>44.6</u>
Diffusion Models	SymmFlow	(SD2.1)	LSTI	39.6
	FlowSeg (Ours)	(PixNerd)	IN-1k	<b>44.9</b>

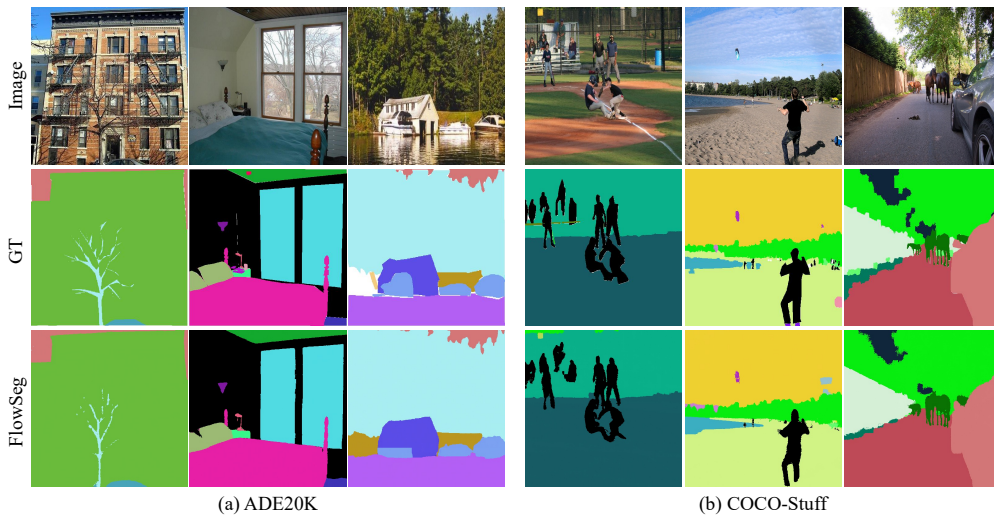


Figure 3: Visualization of segmentation results on (a) ADE20K and (b) COCO-Stuff datasets. Color white in the ground truth (GT) denotes the ignored regions. As ADE20K and COCO-Stuff datasets have different category cardinality, the same color between (a) and (b) does not necessarily represent the same semantic category.

COCO-Stuff datasets, respectively, surpassing strong discriminative baselines with only ImageNet-1k pretraining.

**Qualitative results.** As shown in Fig. 3, we showcase diverse representative scenarios, spanning indoor to outdoor environments and covering objects at various scales. These visualizations demonstrate that FlowSeg robustly handles complex segmentation tasks across varied contexts.

Furthermore, we compare FlowSeg with SymmFlow, which models the transport from the joint distribution of Gaussian noise and images to segmentation masks. As illustrated in Fig. 4(a), SymmFlow fails to yield deterministic predictions and is qualitatively inferior to our method.

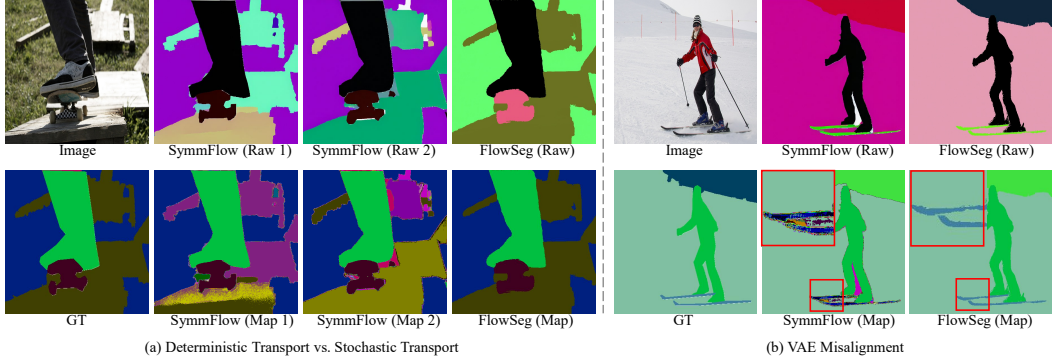


Figure 4: **Visual comparisons between FlowSeg (ours) and SymmFlow (Baseline).** The diffusion model first predicts pseudo-masks (**Raw**), then maps them to the nearest semantic centroids to obtain the final masks (**Map**). (a) Comparison between deterministic (ours) and stochastic modeling: SymmFlow’s predictions vary with random seeds, while ours remain consistent. (b) VAE-based latent space modeling produces masks with similar colors that may not correspond to the correct semantic categories, due to imperfect alignment with pixel-level centroids.

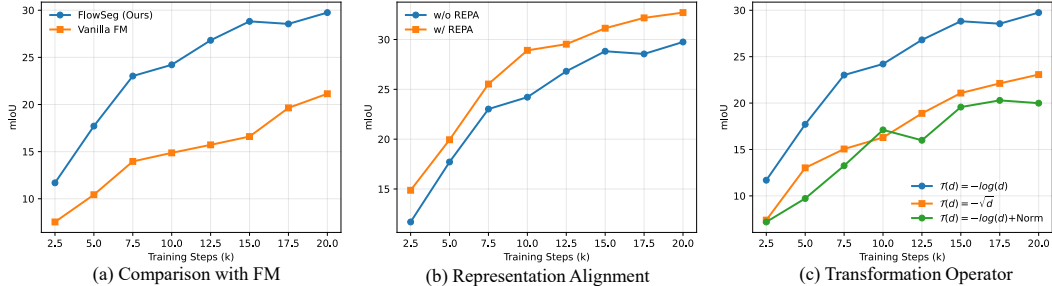


Figure 5: Convergence comparison of different training recipes. (a) FlowSeg vs. vanilla flow matching. (b) Training w/ REPA vs. w/o REPA, (c) Different transformation operators  $\mathcal{T}$ .

### 5.3 Ablation Studies

**Modeling Strategies.** We conduct two main categories of comparisons. From a macroscopic perspective, our method functions as a deterministic flow and employs end-to-end training without a VAE. As shown in Fig. 4 (a), SymmFlow’s involvement of Gaussian noise leads to unstable predictions across different random seeds, which contradicts the requirements of semantic segmentation. In contrast, our FlowSeg consistently achieves stable results due to its deterministic nature. Fig. 4 (b) further demonstrates the advantage of pixel-level end-to-end modeling: since traditional VAE-based methods cannot directly handle pixel-level tasks, they fail to distinguish subtle *pixel-wise* differences in the *latent space*, resulting in raw outputs that appear similar but have highly unstable predicted categories.

For the training objective design, ablation results in Tab. 2 show that using an annealing training target  $\tilde{v}_t = (1 - t)v_t + t(v_t - \nabla\Phi)$ , intended to smooth training, actually degrades performance, possibly because the interpolation weakens discriminative potential. In addition, masking ignored regions proves effective, as it prevents semantically ambiguous areas from affecting optimization. Finally, both x-prediction and v-prediction are viable for model prediction, with only a modest performance difference between them.

**Convergence Comparisons.** We analyze convergence from three perspectives. First, Fig. 5(a) demonstrates that FlowSeg achieves significantly faster convergence from the outset and consistently maintains this advantage throughout training. Building on this architecture, we find that incorporating REPA further boosts performance; as shown in Fig. 5(b), mIoU improves from 29.8 to 32.7 with REPA. Additionally, we evaluate various transformation operators in Fig. 5(c). Our results suggest that gentle operators, such as square root scaling or potential gradient norm reduction, fail to provide sufficient attraction toward target centroids.

Table 2: **Ablation studies of training design choices.** Static  $\tilde{v}_t$  refers to vanilla Eq. 12, while annealing  $\tilde{v}_t$  indicates scaling  $\nabla\Phi$  over time  $t$ . Mask denotes the exclusion of unlabeled regions from optimization. All experiments adopt v-loss.

Prediction	$\tilde{v}_t$	Mask	mIoU
v-pred	Annealing		24.65
v-pred	Static		28.15
v-pred	Static	✓	29.75
x-pred	Static	✓	29.06



Figure 6: Visualization of intermediate states during sampling.

Table 3: Sampling with different steps on the ADE20K dataset. Euler sampler is adopted.

Step	1	2	5	10	20	30	50	100
mIoU	43.47	45.85	46.82	<b>47.1</b>	46.78	46.59	46.13	45.78

**Generative Property Analysis.** FlowSeg inherits the intrinsic characteristics of generative models. Built upon the ODE framework of flow matching, we employ an Euler solver to evaluate performance across various sampling steps (Tab. 3). On the ADE20K dataset, FlowSeg achieves peak performance at 10 steps; however, efficiency-accuracy trade-offs arise, as too few steps lead to discretization errors, while excessive steps may accumulate approximation errors. As visualized in Fig. 6, the intermediate sampling states exhibit smooth evolution trajectories between the image and mask distributions, confirming that our model preserves the continuous mapping properties of flow-based generation.

## 6 Conclusion

This paper explores generative segmentation via flow matching, particularly in high-cardinality segmentation scenarios. We identified two key obstacles to previous methods: gradient vanishing and trajectory traversing. However, these problems are further obscured and entangled by classical latent-space modeling. To tackle these issues, we propose an end-to-end generative segmentation pipeline based on a pixel neural field. Then, we propose a novel vector field reshaping approach that simultaneously solves both problems while maintaining a high gradient near semantic centroids and introducing repulsion in the velocity field. Empirical studies and comprehensive ablations demonstrate significant improvements in convergence speed and final performance over classic flow-matching training recipes, and they closely approach strong discriminative specialists. We hope our research can inspire the community to rethink generative segmentation.

## References

- [1] Niket Agarwal, Arslan Ali, Maciej Bala, Yogesh Balaji, Erik Barker, Tiffany Cai, Prithvijit Chattopadhyay, Yongxin Chen, Yin Cui, Yifan Ding, et al. Cosmos world foundation model platform for physical ai. *arXiv*

- preprint arXiv:2501.03575*, 2025. 1, 3
- [2] Tomer Amit, Tal Shaharabany, Eliya Nachmani, and Lior Wolf. Segdiff: Image segmentation with diffusion probabilistic models. *arXiv preprint arXiv:2112.00390*, 2021. 1, 3
  - [3] Dmitry Baranchuk, Ivan Rubachev, Andrey Voynov, Valentin Khruikov, and Artem Babenko. Label-efficient semantic segmentation with diffusion models. In *ICLR*, 2022. 1, 3
  - [4] Andreas Blattmann, Tim Dockhorn, Sumith Kulal, Daniel Mendelevitch, Maciej Kilian, Dominik Lorenz, Yam Levi, Zion English, Vikram Voleti, Adam Letts, et al. Stable video diffusion: Scaling latent video diffusion models to large datasets. *arXiv preprint arXiv:2311.15127*, 2023. 1, 3
  - [5] Tim Brooks, Aleksander Holynski, and Alexei A Efros. Instructpix2pix: Learning to follow image editing instructions. In *CVPR*, 2023. 1, 3
  - [6] Holger Caesar, Jasper Uijlings, and Vittorio Ferrari. Coco-stuff: Thing and stuff classes in context. In *CVPR*, 2018. 7
  - [7] Francisco Caetano, Christiaan Viviers, Peter HN De With, and Fons van der Sommen. Symmetrical flow matching: Unified image generation, segmentation, and classification with score-based generative models. In *AAAI*, 2026. 7
  - [8] Liang-Chieh Chen, George Papandreou, Iasonas Kokkinos, Kevin Murphy, and Alan L Yuille. Deeplab: Semantic image segmentation with deep convolutional nets, atrous convolution, and fully connected crfs. *TPAMI*, 2017. 1, 3
  - [9] Liang-Chieh Chen, Yukun Zhu, George Papandreou, Florian Schroff, and Hartwig Adam. Encoder-decoder with atrous separable convolution for semantic image segmentation. In *ECCV*, 2018. 7
  - [10] Bowen Cheng, Ishan Misra, Alexander G Schwing, Alexander Kirillov, and Rohit Girdhar. Masked-attention mask transformer for universal image segmentation. In *CVPR*, 2022. 1, 3
  - [11] Bowen Cheng, Alex Schwing, and Alexander Kirillov. Per-pixel classification is not all you need for semantic segmentation. In *NeurIPS*, 2021. 1, 3, 7
  - [12] Patrick Esser, Sumith Kulal, Andreas Blattmann, Rahim Entezari, Jonas Müller, Harry Saini, Yam Levi, Dominik Lorenz, Axel Sauer, Frederic Boesel, et al. Scaling rectified flow transformers for high-resolution image synthesis. *arXiv preprint arXiv:2403.03206*, 2024. 1, 3
  - [13] Yue Fan, Yongqin Xian, Xiaohua Zhai, Alexander Kolesnikov, Muhammad Ferjad Naeem, Bernt Schiele, and Federico Tombari. Toward a diffusion-based generalist for dense vision tasks. *arXiv preprint arXiv:2407.00503*, 2024. 1, 3
  - [14] Zigang Geng, Binxin Yang, Tiankai Hang, Chen Li, Shuyang Gu, Ting Zhang, Jianmin Bao, Zheng Zhang, Han Hu, Dong Chen, et al. Instructdiffusion: A generalist modeling interface for vision tasks. In *CVPR*, 2024. 1, 2, 3, 7
  - [15] Yoav HaCohen, Nisan Chiprut, Benny Brazowski, Daniel Shalem, Dudu Moshe, Eitan Richardson, Eran Levin, Guy Shiran, Nir Zabari, Ori Gordon, et al. Ltx-video: Realtime video latent diffusion. *arXiv preprint arXiv:2501.00103*, 2024. 1, 3
  - [16] Jonathan Ho, Ajay Jain, and Pieter Abbeel. Denoising diffusion probabilistic models. In *NeurIPS*, 2020. 1, 3
  - [17] Yuanfeng Ji, Zhe Chen, Enze Xie, Lanqing Hong, Xihui Liu, Zhaoqiang Liu, Tong Lu, Zhenguo Li, and Ping Luo. Ddp: Diffusion model for dense visual prediction. In *CVPR*, 2023. 1, 3
  - [18] Aliasghar Khani, Saeid Asgari Taghanaki, Aditya Sanghi, Ali Mahdavi Amiri, and Ghassan Hamarneh. Slime: Segment like me. In *ICLR*, 2024. 1, 3
  - [19] Diederik P Kingma and Max Welling. Auto-encoding variational bayes. *arXiv preprint arXiv:1312.6114*, 2013. 3
  - [20] Neehar Kondapaneni, Markus Marks, Manuel Knott, Rogério Guimaraes, and Pietro Perona. Text-image alignment for diffusion-based perception. In *CVPR*, 2024. 1, 3
  - [21] Hsin-Ying Lee, Hung-Yu Tseng, and Ming-Hsuan Yang. Exploiting diffusion prior for generalizable dense prediction. In *CVPR*, 2024. 1, 2, 3
  - [22] Tianhong Li and Kaiming He. Back to basics: Let denoising generative models denoise. *arXiv preprint arXiv:2511.13720*, 2025. 3
  - [23] Chen Liang, Wenguan Wang, Jiaxu Miao, and Yi Yang. Gmmseg: Gaussian mixture based generative semantic segmentation models. In *NeurIPS*, 2022. 3
  - [24] Weifeng Lin, Xinyu Wei, Renrui Zhang, Le Zhuo, Shitian Zhao, Siyuan Huang, Huan Teng, Junlin Xie, Yu Qiao, Peng Gao, et al. Pixwizard: Versatile image-to-image visual assistant with open-language instructions. In *ICLR*, 2025. 1, 3, 7
  - [25] Yaron Lipman, Ricky TQ Chen, Heli Ben-Hamu, Maximilian Nickel, and Matt Le. Flow matching for generative modeling. In *ICLR*, 2023. 2, 3
  - [26] Qiang Liu. Rectified flow: A marginal preserving approach to optimal transport. *arXiv preprint arXiv:2209.14577*, 2022. 2
  - [27] Xingchao Liu, Chengyue Gong, and Qiang Liu. Flow straight and fast: Learning to generate and transfer data with rectified flow. In *ICLR*, 2023. 3, 4
  - [28] Xingchao Liu, Xiwen Zhang, Jianzhu Ma, Jian Peng, et al. InstafLOW: One step is enough for high-quality diffusion-based text-to-image generation. In *ICLR*, 2024. 3

- [29] Jonathan Long, Evan Shelhamer, and Trevor Darrell. Fully convolutional networks for semantic segmentation. In *CVPR*, 2015. 1, 3
- [30] Dustin Podell, Zion English, Kyle Lacey, Andreas Blattmann, Tim Dockhorn, Jonas Müller, Joe Penna, and Robin Rombach. Sdxl: Improving latent diffusion models for high-resolution image synthesis. In *ICLR*, 2024. 1, 3
- [31] Lu Qi, Lehan Yang, Weidong Guo, Yu Xu, Bo Du, Varun Jampani, and Ming-Hsuan Yang. Unigs: Unified representation for image generation and segmentation. In *CVPR*, 2024. 1, 3
- [32] Robin Rombach, Andreas Blattmann, Dominik Lorenz, Patrick Esser, and Björn Ommer. High-resolution image synthesis with latent diffusion models. In *CVPR*, 2022. 1, 3, 7
- [33] Olaf Ronneberger, Philipp Fischer, and Thomas Brox. U-net: Convolutional networks for biomedical image segmentation. In *MICCAI*, 2015. 1, 3
- [34] Jiaming Song, Chenlin Meng, and Stefano Ermon. Denoising diffusion implicit models. In *ICLR*, 2021. 1
- [35] Yang Song, Jascha Sohl-Dickstein, Diederik P Kingma, Abhishek Kumar, Stefano Ermon, and Ben Poole. Score-based generative modeling through stochastic differential equations. In *ICLR*, 2021. 1
- [36] Wouter Van Gansbeke and Bert De Brabandere. A simple latent diffusion approach for panoptic segmentation and mask inpainting. *arXiv preprint arXiv:2401.10227*, 2024. 1, 3
- [37] Chaoyang Wang, Xiangtai Li, Henghui Ding, Lu Qi, Jiangning Zhang, Yunhai Tong, Chen Change Loy, and Shuicheng Yan. Explore in-context segmentation via latent diffusion models. *arXiv preprint arXiv:2403.09616*, 2024. 1, 3
- [38] Chaoyang Wang, Xiangtai Li, Lu Qi, Henghui Ding, Yunhai Tong, and Ming-Hsuan Yang. Semflow: Binding semantic segmentation and image synthesis via rectified flow. In *NeurIPS*, 2024. 1, 2, 3
- [39] Mengyu Wang, Henghui Ding, Jun Hao Liew, Jiajun Liu, Yao Zhao, and Yunchao Wei. Segrefiner: Towards model-agnostic segmentation refinement with discrete diffusion process. In *NeurIPS*, 2023. 1, 3
- [40] Shuai Wang, Ziteng Gao, Chenhui Zhu, Weilin Huang, and Limin Wang. Pixnerd: Pixel neural field diffusion. *arXiv preprint arXiv:2507.23268*, 2025. 3, 7
- [41] Enze Xie, Wenhai Wang, Zhiding Yu, Anima Anandkumar, Jose M Alvarez, and Ping Luo. Segformer: Simple and efficient design for semantic segmentation with transformers. In *NeurIPS*, 2021. 7
- [42] Guangkai Xu, Yongtao Ge, Mingyu Liu, Chengxiang Fan, Kangyang Xie, Zhiyue Zhao, Hao Chen, and Chunhua Shen. What matters when repurposing diffusion models for general dense perception tasks? *arXiv preprint arXiv:2403.06090*, 2024. 1, 3
- [43] Yifeng Xu, Zhenliang He, Meina Kan, Shiguang Shan, and Xilin Chen. Jodi: Unification of visual generation and understanding via joint modeling. *arXiv preprint arXiv:2505.19084*, 2025. 2
- [44] Lehan Yang, Jincen Song, Tianlong Wang, Daiqing Qi, Weili Shi, Yuheng Liu, and Sheng Li. Vrmddiff: Text-guided video referring matting generation of diffusion. *arXiv preprint arXiv:2503.10678*, 2025. 1
- [45] Sihyun Yu, Sangkyung Kwak, Huiwon Jang, Jongheon Jeong, Jonathan Huang, Jinwoo Shin, and Saining Xie. Representation alignment for generation: Training diffusion transformers is easier than you think. In *ICLR*, 2025. 7
- [46] Yongsheng Yu, Wei Xiong, Weili Nie, Yichen Sheng, Shiqiu Liu, and Jiebo Luo. Pixeldit: Pixel diffusion transformers for image generation. *arXiv preprint arXiv:2511.20645*, 2025. 3
- [47] Yuhui Yuan, Xilin Chen, and Jingdong Wang. Object-contextual representations for semantic segmentation. In *ECCV*, 2020. 7
- [48] Hengshuang Zhao, Jianping Shi, Xiaojuan Qi, Xiaogang Wang, and Jiaya Jia. Pyramid scene parsing network. In *CVPR*, 2017. 1, 3
- [49] Wenliang Zhao, Yongming Rao, Zuyan Liu, Benlin Liu, Jie Zhou, and Jiwen Lu. Unleashing text-to-image diffusion models for visual perception. In *ICCV*, 2023. 1, 3
- [50] Bolei Zhou, Hang Zhao, Xavier Puig, Sanja Fidler, Adela Barriuso, and Antonio Torralba. Scene parsing through ade20k dataset. In *CVPR*, 2017. 7